Thermal Parameters Influence Assessed by Electrochemical Impedance Spectroscopy on a $Ni_{50}Ti_{48}Nb_2$ Shape Memory Alloy

IOANA ARINA GHERGHESCU[1], DANIELA IONITA[2], SORIN CIUCA[1], RUXANDRA ELENA DUMITRESCU[1]*

[1] Politehnica University of Bucharest, Materials Science and Engineering Faculty, Department of Materials Science and Physical Metallurgy, 313 Splaiul Independenței, 060042 Bucharest, Romania

[2] Politehnica University of Bucharest, Faculty of Applied Chemistry and Materials Science, 313 Splaiul Independentei, 060042 Bucharest, Romania

This paper presents some electrochemical impedance spectroscopy research results concerning the corrosion resistance of a shape memory $Ni_{50}Ti_{48}Nb_2$ alloy. This one was previously studied by SEM and DSC [1,2] but some new research features had to be made clear in order to be able to explain its electrochemical corrosion behavior. The chemical composition $Ni_{50}Ti_{48}Nb_2$ was chosen in order to obtain a shape memory alloy having a wider hysteresis than equiatomic NiTi, for the purpose of achieving a better thermomechanical stability. Cryogenic applications are aimed. After processing the cast ingot, two samples, S1 and S2, were further annealed at 800°C/12 h and, respectively, at 900°C/12h. Scanning electron micrographs together with the chemical elements mapping results were obtained. They were related to the previous results concerning the informations on the structure of the different phases found in this NiTiNb alloy: austenite, martensite and secondary phases, as well as some primary compounds [1,2]. Considering the size and shape of the complex precipitate particles of NiTiNb in the two differently heat treated samples, these were found responsible for some changes in the transformation temperatures [3] but the electrochemical corrosion behavior of the alloy seems to be influenced to a lesser extent by the heat treatments. Both samples exhibit good values of corrosion resistance, however S2 shows better values than S1. Thus lower transformation temperatures and a slightly better corrosion resistance make the $Ni_{50}Ti_{48}Nb_2$ alloy annealed at 900°C/12h subsequently submitted to thermal cycling to be the right choice for producing couplings in the cryogenic industry.

Keywords: $Ni_{50}Ti_{48}Nb_2$ shape memory alloy, scanning electron microscopy, electrochemical impedance spectroscopy

The issue of increasingly acute environmental pollution requires finding new technological solutions in terms of industrial installations and components that come into contact with air or seas and oceans water.

Submarine pipelines must be designed for fluids transportation at high pressure. The pipe walls are made from high-yield strength steel (350-500 Mpa), exhibiting also good weldability.

In the petroleum industry leaks are unacceptable; the pipelines are subject to internal pressures in the order of 10 MPa, thus the segments are joined by welding. Mechanical joints are also used. Moreover, it was found that a NiTi shape memory alloy fitting system is a cheaper and easier solution when pipes need to fit as compared to conventional couplings methods such as welding.

By now NiTi alloy couplings have proved over 35 years of reliability, no leaks being reported. They are even stronger than the pipes that are joined. Such a feature is of great importance in aeronautics, naval industry and high importance fluid transportation through pipelines.

In this perspective it is possible that further research, development and installation of couplings made of other NiTiNb shape memory alloys than thoses used so far (such as $Ni_{47}Ti_{44}Nb_9$) become an interesting solution for assembling underwater pipelines, as long as they exhibits a good corrosion resistance in inorganic salt solutions.

A shape memory $Ni_{50}Ti_{48}Nb_2$ alloy was chosen in order to provide a wider hysteresis than the well-known equiatomic NiTi, that leads to a better thermomechanical stability, thus to a higher reliability [3,4]. Apart from the need to test its corrosion resistance, such a material should have stable solid state transformation temperatures making it suitable for an application like cryogenic couplings. This last requirement may be achieved by thermal cycling performed on a device being formerly heat treated at a specific temperature. Afterwards, electrochemical corrosion tests were performed.

Experimental part

The raw materials used in producing the NiTiNb alloys were: vacuum remelted Ti (Ugine - 99.99%), electrolytic Ni (INCO - 99.98%) and TiNb master alloy, having 44 wt% titanium.

All raw materials were grinded in order to remove the oxide layers and were also chemically cleaned in a 1/3V. HF + 2/3V. HNO_3 solution and finally in acetone.

The materials were melted in a high frequency induction furnace (induction heating frequency 0.5 MHz, power 25 kW). This furnace allows the alloy to be produced in neutral atmosphere, in a copper pipe continuously refreshed with water that ensures, on one hand, a satisfactory homogeneization degree due to the electromagnetical induction, and on the other hand, a high rate cooling which prevents a rough segregation inside the ingots.

The ingot had an approximately cylindrical shape (6 mm radius and 50 mm length) and 40 gr. weight.

A homogenizing annealing at 900°C/48 h was performed. Prior to all deformation, the ingot was subsequently chemically cleaned in a (1 V. H_2O_2 + 1V. HNO_3 + 1V. HF) acid solution.

After a hot rolling at 800°C up to a section of about 40 mm^2 the heating temperature was lowered at 750°C in order to avoid titanium loss by oxydation. The ingots were further on cold rolled, with prior heatings at 750°C/5 min before every cold rolling passage.

*email: ruxandraelenadumitrescu@gmail.com; Phone: +40723344813

Two samples, S1 and S2, were further annealed at 800°C/12 h and, respectively, at 900°C/12h. Differences regarding their transformation temperatures, microstructure and corrosion resistance were to be found and evaluated.

A former study showed the results obtained when performing differential scanning calorimetry (DSC) that enables one to find the transformation temperatures of the alloy which assign it for a required application [3]. Some previous electron microscopy research of the as-cast $Ni_{50}Ti_{48}Nb_2$ alloy was also conducted [1,2].

The tests to be performed on NiTiNb samples are, as follows:

-Scanning electron microscopy (SEM) of the $Ni_{50}Ti_{48}Nb_2$ alloy in order to establish changes in the alloy structure precipitates morphollogy; their chemical composition was previously checked [1,2].

-Electrochemical corrosion tests are aimed to establish if one of the two above mentioned annealings provides a better corrosion resistance of the alloy than the other one.

Results and discussions

Scanning electron microscopy (SEM)

Among the NiTiNb alloys, $Ni_{47}Ti_{44}Nb_9$ was the first alloy to be intensively studied [4-6] . Other alloys belonging to the NiTiNb class are scarcely described.

As for the $Ni_{47}Ti_{44}Nb_9$ alloy, its microstructure reveals the presence of niobium-rich precipitates in the NiTi equiatomic solid solution matrix. These precipitates are insoluble on heating up to 1100°C. For longer holding times, the precipitates increase [6]. These are therefore compound particles formed at high temperatures, probably during solidification (primary solid particles of a compound). They exhibit a chemical composition very close to NbTi system β phase, containing ~ 80% Nb [6].

Concerning the 2% Nb alloy, these compounds are not found, in agreement with the equilibrium diagrams of the NbNi [7] and NbTi [8] systems. Biphasic areas matrix + compounds were obtained. X-ray diffraction concerning Nb distribution clearly shows the existence of a higher niobium percentage in some of the compounds found in $Ni_{50}Ti_{48}Nb_2$ alloy [1,2].

The compounds that are found in the microstructure are: one of them is from the NiTi system - Ti_2Ni - and also compounds based on solid solutions of Ni, Ti and Nb such as $Ni_{53,5}Ti_{42}Nb_{4,5}$ or $Ni_{46}Ti_{32,5}Nb_{21,5}$ [1,2] were identified. These two Nb-rich compounds are to be found on all samples: as-cast, hot-rolled and annealed [1,2].

The examination of these particles was extremely difficult, because of their very weak coherence with the matrix, or even complete lack of coherence. All performed etching methods pulled out the compounds from the matrix, thus what is presumed to be precipitates on the SEM images are most of the time cavities wherefrom these where pulled out.

The compounds distributed along the grain boundaries belong to an eutectic consisting in a NiTiNb solid solution, Ti_2Ni compound particles and also of Nb – rich compounds.

A previous study showed microstructures of as-cast and hot-rolled samples. The morphollogy of some idiomorphic crystals intercepted on the secondary electron image suggested their cubic lattice symmetry [1,2]. Also, a cellular eutectic structure was found on SEM images; niobium has a higher atomic number as against nickel and titanium, thus may be seen as a light - coloured network surrounding darker NiTiNb solid solution grains [1,2]. Considering the hot-rolled sample, changes when compared with the as-cast sample were reported: the eutectic morphollogy was partially modified by eutectic cells shattering. The compound crystals are somewhat rounded, nevertheless conserving a distribution that suggest the former grain boundaries. The X-ray mapping showed a regular distribution for Ni, Ti and Nb on the whole examined surface, which confirms that the compounds were pulled out by etching.

Further on are presented the SEM microstructures and Ni, Ti, Nb EDS elemental mapping images of samples S1 and S2, heat treated at 800°C/12h and, respectively, at 900°C/12h.

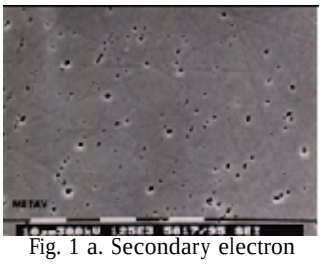

Fig. 1 a. Secondary electron image showing Nb-rich compounds, etching with HF, sample S1.

Fig. 1 b. EDS elemental mapping images of Nb, sample S1.

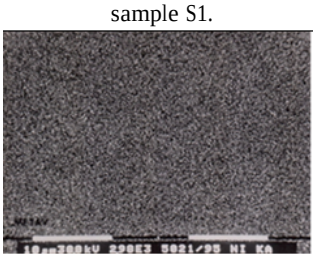

Fig. 1 c. EDS elemental mapping images of Ni, sample S1.

Fig. 1 d. EDS elemental mapping images of Ti, sample S1

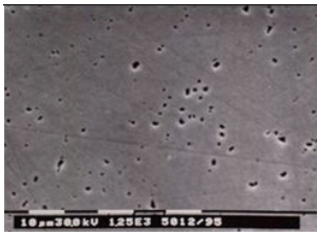

Fig. 2 a. Secondary electron image showing Nb-rich compounds, etching with HF, sample S2.

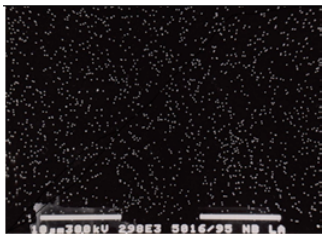

Fig. 2 b. EDS elemental mapping images of Nb, sample S2.

Fig. 2 c. EDS elemental mapping images of Ni, sample S2.

Fig. 2 d. EDS elemental mapping images of Ti, sample S2.

Regarding the samples S1 and S2 SEM microstructures, their crystals form and distribution are not radically changed as compared to the hot-rolled sample [1] ; they continue to be suggestive of the former grain boundaries. Some of the particles are found inside the grains.

The explanation concerning the changes in the distribution of the compounds may be given by assuming the existence of a solvus surface of solubility variation in the solid state such as when heating, some of the Nb - rich compounds are partially dissolved; on further cooling they re-precipitate as finer crystals with a different distribution

in contrast to the originary one. The Ti_2Ni compound may also be found inside the grains and not along the boundaries of the cellular structure, due to the fact that they are not precipitating along a solvus surface, they are intermetallic by their nature, as seen in NiTi equilibrium diagram [9]. Some idiomorphic crystals are still found in the heat treated samples, S1 and S2. They are also able to grow by diffusion at higher temperatures and longer holding times [6].

Most of the compounds are found to have slightly larger sizes in the S2 heat treated sample when comparing to S1 as one can see in figures 1a and 2a.

Differential Scanning Calorimetry (DSC)

Even if the presentation of a research on differential scanning calorimetry - DSC - is not the main purpose of this paper, some prior results must be reminded; they will allow a better conjunction between the microstructural features and the electrochemical corrosion behavior of the two heat treated samples, S1 and S2.

Several aspects are to be reminded, concerning the transformation temperatures determined by DSC and their shifting due to thermal cycling: in a previous study [3] the same samples S1 and S2 were submitted to thermal cycling by means of DSC.

Several changes in the critical points were reported. After 24 cycles applied on sample S1, M_s dropped from -32 to -53°C , A_s from -31 to -50°C and A_f from +14 to +4°C. For sample S2, after 20 cycles, M_s dropped from -49 to -55°C , A_s from -32 to -40°C and A_f from +27 to 0°C [3].

The hysteresis values for S1 sample were, succesively: 47, 53, 53, 51, 49°C and those for the S2 sample were: 50, 61, 64, 67, 72°C. One may observe that hysteresis values for sample S1 vary around 50 degrees without exhibiting a linear tendency; as for sample S2, they are constantly rising, from 50 to 72°C [3].

No matter the NiTi alloy, the shift of the critical points may be ascribed to the material microstructure, to defects such as dislocations and stacking faults and to some changes in the atomic disposition of ordered NiTi. It was found that there is an upper limit of the whole number of the transformation – induced defects present in the NiTi alloys. After applying a large number of transformation cycles, the amount of the induced defects will be the same as that of defects annihilated during the transformation [10]. But before reaching an equilibrium configuration, the defects induced by the transformation may be more or less numerous than the number of defects annihilated by the same transformation, thus the transformation temperatures values will vary.

It is to be mentioned that a very small shifting effect of the transformation temperatures was found on equiatomic NiTi by thermal cycling [11].

Considering the $Ni_{50}Ti_{48}Nb_2$, at least one of the compounds mentioned above is growing by coalescence when applying a heat treatment at higher temperature (900 vs. 800°C). The fact that among all compounds there is a secondary precipitate being submitted to a coalescence - dissolution kinetic is sustained by their cellular distribution as it was previously presented [1].

The most important feature needed to be explained is related to the differences between the critical points obtained on the two differently heat treated samples S1 and S2.

Every single compound particle is involved in the kinetics of the martensitic and reverse transformation. The sample annealed at 900°C/12 h will have a lower number of (larger) compounds as against the sample annealed at 800°C/12 h, this feature being related to the fact that some of the particles grew by coalescence. Their total interface matrix-compound, prone to generate nucleation centers, will be smaller. The whole quantity of defects, mostly dislocations, susceptible of being involved as nucleation centers in the transformation, will be smaller. Thus the driving force of the transformation will need to be higher, so the M_s point corresponding to the sample annealed at 900°C/12h will be lower [3].

Considering further on the martensitic transformation, the martensite twins need to produce some local microdeformations of the compounds in order to overcome the energy barrier represented by these particles. For sake of comparison, when a deformation of the material takes place, M_s will raise and be denominated M_d. When increasing the number of cycles, this effect will be less important, leading to a shift of the transformation temperatures to lower values, up to a point where a stable configuration is reached and transformation temperatures vary no more.

The whole microstructure stabilization tendency may also explain the shifting to lower values of A_s and A_f. On the one hand, the compounds surfaces are deformed by martensite twins when the first cooling cycle is applied; the reverse transformation must overcome this deformations but from the second cycle to the last, the compound surfaces will be more and more shattered and their involvement in the transformation progressively reduced. On the other hand, the configuration of the whole quantity of defects tends to an equilibrium one; A_s and A_f will thus shift to lower values because of a smaller driving force needed to initiate and complete the transformation.

Usually cryogenic couplings made of such a material are expanded in the pre-final form in liquid nitrogen, the very low M_s and M_f temperatures requiring it. An A_f point next to 0°C guarantees the reliability in service. Sample S2 exhibit even better temperatures from this point of view, a complete austenitic transformation being accomplished at 0°C. Hysteresis values are also better for sample S2; they are constantly rising from 50 to 72°C, when increasing the number of the applied thermal cycles [3].

Estimation of corrosion resistance of the $Ni_{50}Ti_{48}Nb_2$ alloy by electrochemical impedance spectroscopy.

For the electrochemical impedance spectroscopy (EIS) measurements, the two $Ni_{50}Ti_{48}Nb_2$ samples previously annealed under 800°C/12h and respectively 900°C/12h were exposed to NaCl 3% solution at room temperature for 300 h. A standard three-electrode cell arrangement was used in the experiments. The working electrode was the NiTiNb alloy, the counter electrode was a platinum mesh and the reference electrode was a saturated calomel electrode (SCE). The impedance data were obtained at the open-circuit potential using an Autolab 302 Potentiostat/Galvanostat. The impedance spectra were acquired in the frequency range of 10^{-2} - 10^5Hz. The applied amplitude of the AC potential was of 10mV.

The passivation mechanism consists in the formation of a passive film with two layers: an inner compact layer also termed a barrier layer, giving the alloy a good resistance and a porous outer layer formed at the interface with the electrolyte, through which light passive dissolution processes are carried out.

Further on electrochemical impedance spectroscopy (EIS) plots for different holding times and the electrical parameters obtained from the impedance data, for both S1 and S2 samples (fig. 3).

Q_1, Q_2 are the constant phase elements (CPE_1, CPE_2) and $\mathbf{n_1}$ and $\mathbf{n_2}$ are the CPE exponents given by circuit fitting.

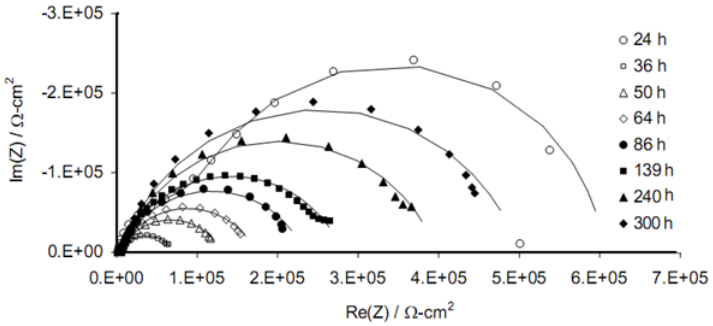

Fig. 3. Electrochemical impedance spectroscopy (EIS) plots for different holding times, sample S1

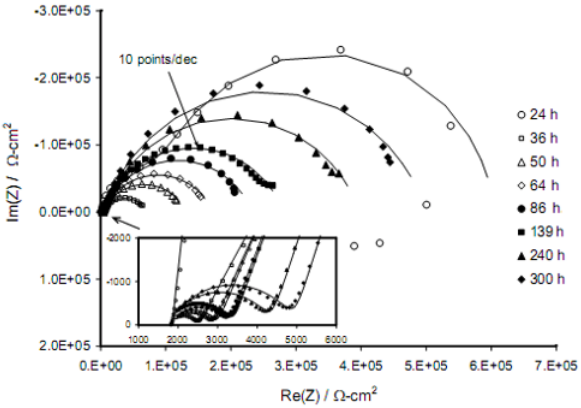

Fig. 4. Electrochemical impedance spectroscopy (EIS) plots for different holding times, sample S2

Table 1

THE ELECTRICAL PARAMETERS OBTAINED FROM THE IMPEDANCE DATA, SAMPLE S1 (800°C/12 h)

Time (h)	R_s [Ω]	R_1[kΩ]	Q_1 (μF/cm²)	n_1	R_2 [kΩ]	Q_1 (μF/cm²)	n_2	i_{corr} μA/cm²
25	17.4	1.4	44.3	0.81	4.92	148	0.90	0.06
36	17.2	0.025	16.6	0.66	0.52	660	0.78	1.59
50	16.5	0.026	14.5	0.62	1.08	556	0.73	0.49
64	17.3	0.030	16	0.63	1.5	448	0.75	0.39
86	17.4	0.034	13.5	0.66	1.6	400	0.75	0.34
96	17.2	0.038	12.2	0.64	1.8	356	0.76	0.28
139	17.9	0.043	10.8	0.65	2.0	322	0.77	0.26
240	17.2	0.041	9.85	0.63	3.2	288	0.80	0.19
300	17.8	0.043	6.72	0.66	3.4	226	0.81	0.16

Table 2

THE ELECTRICAL PARAMETERS OBTAINED FROM THE IMPEDANCE DATA, SAMPLE S2 (900°C/12 h)

Timp (h)	R_s [Ω]	R_1[kΩ]	Q_1 (μF/cm²)	n_1	R_2 [kΩ]	Q2 (μF/cm²)	n_2	i_{corr} μA/cm²
25	18.5	140	45	0.91	4.5	184	0.93	0.08
36	18.2	10.4	9.66	0.56	0.9	566	0.68	0.59
50	17.5	12.2	6.45	0.62	1.2	456	0.75	0.42
64	18.3	13.8	5.6	0.63	1.8	342	0.74	0.34
86	18.4	15.8	4.35	0.61	2.2	280	0.75	0.26
96	18.2	15.5	3.72	0.64	2.1	256	0.76	0.18
139	16.9	19.2	2.98	0.62	2.9	222	0.76	0.21
240	17.5	26.8	2.85	0.63	3.8	198	0.78	0.16
300	17.6	32.5	2.72	0.63	4.2	165	0.80	0.11

The corrosion current exhibit good values as a whole, even better (lower) for sample S2, indicating that the shape

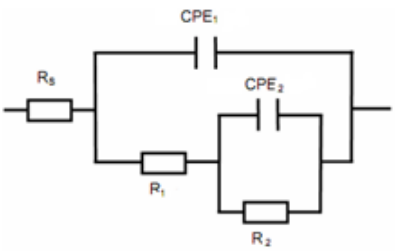

Fig. 5. Electrochemical equivalent circuit: R_s- electrolyte resistance; R_1, R_2 - polarization resistances; Q_1 (CPE_1), Q_2 (CPE_2) - constant phase element.

memory $Ni_{50}Ti_{48}Nb_2$ alloy exhibits a good corrosion resistance.

The impedance response for the present passive systems is interpreted with the aid of the analog equivalent circuit shown in figure 5.

In this model, R_s corresponds to the resistance of the electrolyte. R_1 and R_2 are the polarization resistances of the outer porous and respectively inner barrier layers.

For the mathematical analysis of impedance diagrams, a constant phase element, CPE, was used instead of an *ideal* capacitor and CPE_1, CPE_2 are deûned as capacitances of porous and barrier layers, respectively. The parameter CPE generally denotes the impedance of a phase element as $CPE = [C(\varphi)^n]^{-1}$ (where ω is frequency and $-1 \leq n \leq 1$) and corresponds to the capacitance ($1Hz < F < 1$ kHz).

The **n** values of nearly one suggest that the behavior of such a layer approached that of an ideal capacitor.

All impedance parameters are to be found in table 1 and table 2. The resistance and capacitance values of the porous and barrier layers are given in table 1 and table 2 for samples S1 and S2, respectively. According to the proposed model, the passive film consists of two layers, the inner barrier layer, whose resistance value R_2 is significantly larger than the value associated to the outer porous layer R_1, as shown in table 1 and 2.

In the S1 case the results indicate that the protection provided by the passive layer is predominantly due to the inner layer.

Concerning S2 sample, the protection effect is also due to a better corrosion resistance of the porous layer.

The differences of the polarization resistances R_1 and R_2 between the two samples are rather small. However these differences are noticeable and this can be ascribed to the fact that the passive film formed on these alloys is

submitted to changes when applying different heat treatment temperatures. The fact that sample S2, annealed at 900°C/12 h, exhibits a slightly better corrosion resistance is due, as well as transformation temperatures shifting, to a lower number of larger compounds grown by coalescence as compared to sample S1 annealed at 800°C/12 h. Their total interface matrix-compound will be smaller. The whole quantity of defects, mostly dislocations, will thus be smaller, influencing the electrochemical corrosion processes and improving the corrosion resistance.

Conclusions

A shape memory NiTiNb alloy having a rather small Nb concentration such as $Ni_{50}Ti_{48}Nb_2$ was found to have low transformation temperatures, thus making it adequate for being used in cryogenic coupling.

Samples S1 and S2 of a shape memory $Ni_{50}Ti_{48}Nb_2$ alloy were submitted to two different annealing heat treatments. Significantly differences were found in their critical points (transformation temperatures) [3]. Some changes were also reported regarding their microstructures and, at a lesser magnitude, in their corrosion resistance characteristic parameters.

The phenomena were explained on the basis of structural changes in size and also shape of the precipitates found in the alloy structure, as a consequence of being submitted to annealing heat treatments at two different temperatures, 800°C/12 h and, respectively, at 900°C/12h.

From one heat treatment to the other, some of the precipitates were changed in size by a coalescence process, thus a smaller number of larger particles will have a smaller total sum of boundary surfaces containing a smaller amount of defects, which implies a lower boundary-associated stress level. Idiomorphic crystals are also found in the heat treated samples, S1 and S2 [1]. They are also able to grow by diffusion at high temperatures [6] and long holding times and produce the same effect when it comes to changes in transformation temperatures and corrosion resistance properties.

Consequently, a better corrosion resistance was found for the sample annealed at 900°C/12h. Considering also the lower transformation temperatures of sample S2 as against S1 one may conclude that a $Ni_{50}Ti_{48}Nb_2$ alloy, previously annealed at 900°C/12h and submitted to thermal cycling is a better choice for cryogenic couplings production.

References

1.GHERGHESCU, I.A., U. Politeh. Buch. Ser. B, **61**, Issue 1-2, 1999, p.181.

2.GHERGHESCU, I., CIUCA, S., Bulletin of the Polytechnic Institute of Jassy, Romania, Vol. LI (LV), 2005, p.213

3.GHERGHESCU, I.A., CIUCA, S., JICMON, G.L., DUMITRESCU, R.E., BRANZEI, M., Rev. Chim. (Bucharest), **68**, no. 5, 2017, p. 991.

4.DUERIG, T.W., MELTON, K.N., Proc. ESOMAT 1989 - Ist European Symposium on Martensitic Transformations in Science and Technology, (eds.) E. Hornbogen, N. Jost, 1989, p. 191.

5.MELTON, K.N., PROFT, J.L., DUERIG, T.W., Proc. ESOMAT 1989 - East European Symposium on Martensitic Transformations in Science and Technology, (eds.) E. Hornbogen, N. Jost, 1989, p. 169.

6.ZHAO, L.C., DUERIG, T.W., WAYMAN, C.M., Proc. MRS Int'l Meeting on Advanced Materials Shape Memory Materials, 9, 1989, p. 175.

7.*** ASM Handbook, Vol.3, Alloy Phase Diagrams, 1992, p.304

8.*** ASM Handbook, Vol.3, Alloy Phase Diagrams, 1992, p.307

9.*** ASM Handbook, Vol.3, Alloy Phase Diagrams, 1992, p.319

1o.MATSUMOTO, H., Physica B, **334** , Issue 1 - 2, 2003, p.115.

11.AIROLDI, G., BELLINI, G., DI FRANCESCO, C., J. Phys. F: Met. Phys., **14**, Issue 8, 1984, p.1985

Manuscript received: 9.11.2017